

Simulation of DGSOI MOSFETs with a Schrödinger-Poisson Based Mobility Model

Andreas SCHENK^{†a)} and Andreas WETTSTEIN^{††}, *Nonmembers*

SUMMARY A TCAD implementation of a quantum-mechanical mobility model in the commercial device simulator DESSIS-ISE is presented. The model makes use of an integrated 1D Schrödinger-Poisson solver. Effective mobilities μ_{eff} and transfer characteristics are calculated for DGSOI MOSFETs with a wide range of silicon film thickness t_{Si} and buried-oxide thickness t_{box} . It is shown that the volume-inversion related enhancement of μ_{eff} for $t_{\text{Si}} \approx 10$ nm is bound to symmetrical DGSOIs, whereas SIMOX based devices with thick buried oxides limit μ_{eff} to the bulk value. The still immature technology makes a conclusive comparison with experimental data impossible.

key words: device simulation, DGSOI MOSFET, channel mobility, quantum effects, Schrödinger-Poisson solver

1. Introduction

Ultra-thin DGSOI transistors are considered as one of the most promising devices for future VLSI. Besides improvements in the sub-threshold behavior (reduced short-channel effects) and a reduction of junction capacitance, a theoretical enhancement of the channel mobility was found by some authors [1]–[4]. All these effects result in higher speed, higher packing density, and lower power dissipation.

Because there is a variety of mutual effects, as quantum-mechanical confinement, sub-band splitting induced change of occupation, and geometry effects from gate oxide thicknesses, a simple analytical model for the channel mobility in DGSOI MOSFETs didn't emerge yet. The latter was either computed as stand-alone mobility model [1], [2], or a Monte Carlo simulator was extended by scattering rates based on explicitly calculated wave functions in the DGSOI channel [3]–[5].

Here, we present a TCAD implementation of a quantum-mechanical mobility model in the commercial device simulator DESSIS-ISE. The model based on an integrated Schrödinger-Poisson solver is applied to DGSOI MOSFETs with a range of silicon slab thickness t_{Si} and buried-oxide thickness t_{box} . The main finding is that the theoretical enhancement of effective mobility and on-current at $t_{\text{Si}} \approx 10$ nm is bound to

comparable thicknesses of buried and front oxides. If $t_{\text{box}} \approx 100 \times t_{\text{ox}}$, as e.g. in the case of SIMOX wafers, the volume-inversion related increase of the mobility completely vanishes.

Details of the transport and mobility model are given in Sect. 2. The simulation results for the effective mobility in symmetrical and asymmetrical DGSOI MOSFETs as well as the simulated transfer characteristics are presented in Sect. 3. In Sect. 4 the simulations are compared with measurements. Conclusions are drawn in Sect. 5.

2. Transport and Mobility Model

The density-gradient model [6], [7] is used in the entire MOSFET which automatically includes the gate quantum-depletion effect [8]. A domain under the front gate covering front oxide, buried oxide, and lowly p-doped (10^{15} cm^{-3}) silicon slab (see Fig. 1), is subject to the 1D Schrödinger solver which yields all information (eigenenergies, envelope wave functions Ψ_N in quantization direction) needed for the computation of the channel mobility. The Schrödinger equation is solved with the density-gradient potential, hence self-consistency with the Poisson equation is only approximate. This 'hybrid' approach has proven to improve convergence at larger drain currents with only little loss of accuracy in potential and electron density. The density-gradient quality of the latter in a symmetrical DGSOI with $t_{\text{Si}} = 5$ nm and $t_{\text{ox}} = t_{\text{box}} = 1.5$ nm is shown in Fig. 2. Details of the density gradient model in the device simulator DESSIS-ISE [9] are described in [6], details of the mobility model can be found in [7].

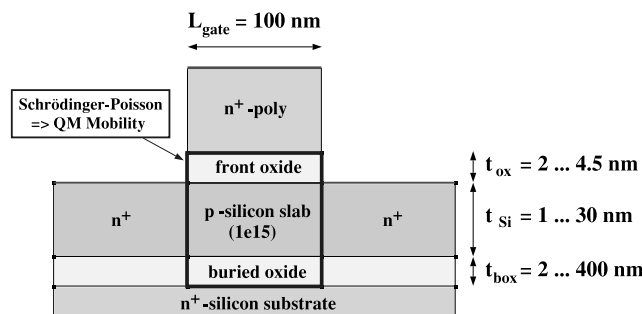


Fig. 1 DGSOI MOSFET cross section with Schrödinger-Poisson window.

Manuscript received September 4, 2002.

Manuscript revised November 4, 2002.

[†]The author is with Institut für Integrierte Systeme, ETH Zürich, Gloriastrasse 35, CH-8092 Zürich, Switzerland.

^{††}The author is with ISE Integrated Systems Engineering AG, Balgriststrasse 102, CH-8008 Zürich, Switzerland.

a) E-mail: schenk@iis.ee.ethz.ch

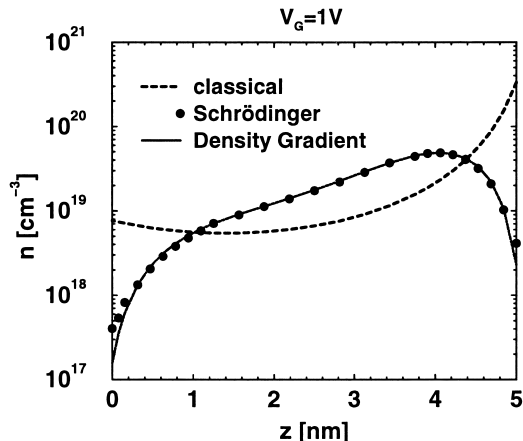


Fig. 2 Electron density across the channel in the center of a DGSOI MOSFET with $t_{\text{Si}} = 5$ nm, $t_{\text{ox}} = t_{\text{box}} = 1.5$ nm, and 80 nm channel length. Comparison between self-consistent Schrödinger-Poisson (symbols), density-gradient (solid), and classical distribution (dashed).

The latter makes use of the relaxation time approximation for acoustic-phonon (ac), inter-valley-phonon (iv), and interface-roughness (IR) scattering. In this approximation the conductivity is expressed in terms of scalar relaxation times $\tau_N[\vec{k}]$,

$$\sigma[z] = \frac{q^2\beta}{2} \sum_N \int \frac{d^2\kappa}{4\pi^2} f[E_{\vec{K}}] (1 - f[E_{\vec{K}}]) \times \bar{v}_N^2[\vec{k}] |\Psi_N[z]|^2 \tau_N[\vec{k}]. \quad (1)$$

The multi-index $N = (n, \nu, \sigma)$ contains the sub-band index n , the valley index ν , and the spin index σ , in order to take account of quantization in z -direction. \vec{K} is a multi-index comprised of N and the wave vector in the xy -plane, \vec{k} . It has to be assumed that the relaxation time $\tau_N[\vec{k}]$ depends only on N and the energy $E = E_N + E_{xy}[\vec{k} = 0]$ with respect to the sub-band bottom. This makes one integration in Eq. (1) feasible to give

$$\sigma[z] = \frac{q^2\beta}{4\pi} \sum_N \frac{m_x^\nu + m_y^\nu}{m_{xy}^\nu \hbar^2} \int_0^\infty dE \frac{E(1 + \alpha E)}{1 + 2\alpha E} \times f[E_N + E] (1 - f[E_N + E]) |\Psi_N[z]|^2 \tau_N[E] \quad (2)$$

with the nonparabolicity factor α . The matrix elements of a scattering operator in a 2D system can be expanded in terms of matrix elements with plane waves, the 3D states usually assumed instead of Bloch states. In the case of a momentum conserving operator \mathcal{M} , the 3D matrix elements transform into

$$\langle \vec{k}'\gamma' | \mathcal{M} | \vec{k}\gamma \rangle = \delta_{\vec{k}-\vec{k}', \vec{q}\gamma\gamma'} M[\vec{q}\gamma\gamma'],$$

where γ labels the state of the system of scatterers (phonons) and $\vec{q}\gamma\gamma'$ the change of the momentum of the latter due to the scattering event. Projecting the

2D states onto the 3D states one obtains

$$\begin{aligned} & \langle \vec{k}'N'\gamma' | \mathcal{M} | \vec{k}N\gamma \rangle \\ & = \delta_{\vec{k}-\vec{k}', \vec{q}\gamma\gamma'} J_{N'N} [q_z^{\gamma\gamma'}] M[\vec{q}\gamma\gamma'], \end{aligned}$$

where the $J_{N'N}$ replace momentum conservation in z -direction

$$J_{N'N} [q_z^{\gamma\gamma'}] = \int dz \exp[-iq_z^{\gamma\gamma'} z] \Psi_{N'}^*[z] \Psi_N[z].$$

As scattering rates depend on the squared modulus of the matrix elements and contain summations over all momenta, the quantity

$$\begin{aligned} \alpha_{N'N} & = \int \frac{dq_z}{2\pi} |J_{N'N}[q_z]|^2 \\ & = \delta_{\sigma\sigma'} \int dz |\Psi_{N'}[z]|^2 |\Psi_N[z]|^2, \end{aligned} \quad (3)$$

the so-called form factor, multiplies the scattering rates of the 2D carrier system. The explicit expressions for the rates of ac and iv scattering as well as the analytical formulas derived for the corresponding relaxation times can be found in Ref. [7].

The roughness responsible for IR scattering is parameterized in the usual way by an amplitude Δ and a spatial correlation length L_{corr}

$$|\Delta[\vec{k}]|^2 = \frac{\Delta^2}{L_x L_y} \frac{\pi L_{\text{corr}}^2}{\sqrt{1 + \vec{k}^2 L_{\text{corr}}^2/2}^3}, \quad (4)$$

which corresponds to an exponential behavior of the spatial autocorrelation of the oxide thickness fluctuations [10]. The fluctuations cause the position of the oxide at point $\vec{z} = (x, y)$ to be shifted from its mean position at $z = 0$ by an amount of $\Delta[\vec{z}]$. This leads to a perturbation of the Hamiltonian $\delta\mathcal{H} \approx \delta\Phi_B + q\delta\phi$, where $\delta\Phi_B$ is the contribution from the band edge jump

$$\begin{aligned} \delta\Phi_B[\vec{z}, z] & = (\Phi_B[0^-] - \Phi_B[0^+]) \\ & \times (\Theta[z] - \Theta[z - \Delta[\vec{z}]]) \end{aligned} \quad (5)$$

and $\delta\phi$ is the first order correction of the electrostatic potential. The latter is self-consistently related to charge fluctuations $\delta\rho[\vec{z}, z]$ via the Poisson equation

$$\nabla\delta\epsilon[\vec{z}, z] \cdot \nabla\phi[z] + \nabla\epsilon[z] \cdot \nabla\delta\phi[\vec{z}, z] = -\delta\rho[\vec{z}, z]. \quad (6)$$

In first-order perturbation theory the induced charge is given by

$$\begin{aligned} \delta\rho[\vec{z}, z] & = q \sum_{\vec{K}\vec{K}'} \Psi_{\vec{K}}^*[\vec{z}, z] \Psi_{\vec{K}'}[\vec{z}, z] \\ & \times \frac{f[E_{\vec{K}}] - f[E_{\vec{K}'}]}{E_{\vec{K}} - E_{\vec{K}'}} \langle K' | \delta\mathcal{H} | K \rangle. \end{aligned} \quad (7)$$

The derivation of matrix elements and relaxation times from Eqs. (4)–(7) is outlined in Ref. [7]. Note that in

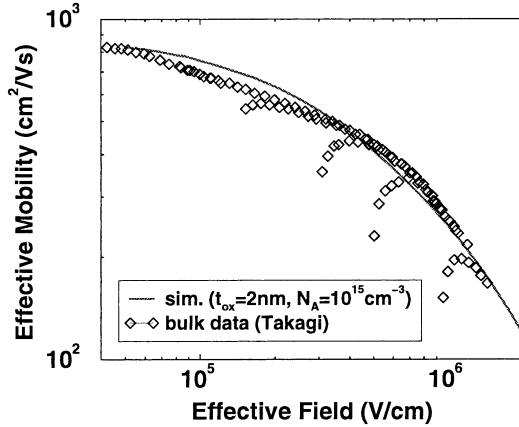


Fig. 3 Measured [12] versus simulated effective mobility in bulk silicon. Parameters: $t_{\text{ox}} = 2 \text{ nm}$, $N_A = 10^{15} \text{ cm}^{-3}$, other parameters as given in Table 1.

Table 1 Parameters for the electron mobility. $D_{\text{int},f}$ and $D_{\text{int},g}$ are the inter-valley deformation potential constants for f- and g-type scattering, respectively.

Quantity	Value	Unit
$\Delta_{1,2}$	0.32	nm
$L_{\text{corr},1,2}$	1.5	nm
α	0.5	$(\text{eV})^{-1}$
$D_{\text{int},g}$	1.0	GeV/cm
$D_{\text{int},f}$	0.2	GeV/cm
D_{ac}/c_1	12	$\mu\text{eVs/cm}$
$\hbar\omega_{\nu\nu'}$	60	meV

virtue of Eqs. (5)–(7) screening of IR scattering is obtained self-consistently by the iteration of the system's first-order response to geometrical fluctuations of the interfaces.

The mobility model neglects Coulomb scattering at dopants in the channel and also at remote charges, therefore it is only reliable in the on-state of the MOSFET, where ionized impurity scattering is screened out. However, impurity scattering in the source/drain regions is taken into account by the common Masetti model [11]. The number of subbands is restricted to 11 in order to allow for routinely simulations. Bulk coupling constants are used which reproduce the universal mobility curve of bulk MOSFETs (see Fig. 3).

The parameters used in this paper are summarized in Table 1. We assume equal IR amplitudes $\Delta_1 = \Delta_2$ at both interfaces and neglect the interdependence of upper and lower IR scattering. In particular, the perturbation of the electrostatic potential caused by the displacement of the interfaces is computed separately for the upper and lower interface. The perturbation is assumed to vanish at the top gate and at $z = \infty$ for the top interface, and at the lower gate and $z = -\infty$ for the bottom interface. For simplicity, the modification of the electron density induced by the displacement of the interfaces and the resulting modification of the electrostatic potential is neglected, that is, screening is

disregarded. This leads to the adjusted IR amplitudes summarized in Table 1 and to the fit for the effective mobility in Fig. 3. As shown by Gamiz et al. in Ref. [5] for a simplified IR perturbation Hamiltonian, the modification of the latter due to the presence of the buried interface leads to an increase of the effective mobility in the IR-dominated range compared to the corresponding Hamiltonian used in bulk situations. As in their work the thickness of the buried oxide was large, such a modification will be different for symmetrical DGSOIs. In the light of the somewhat questionable physical meaning of the commonly used IR perturbation operator and because there are 4 adjustable IR parameters, we did not attempt to follow the line of Ref. [5].

The remaining symbols in Table 1 have the following meaning: $L_{\text{corr},1,2}$ are the auto-covariance lengths of the roughness fluctuations (assumed to be equal for both interfaces), α is the nonparabolicity parameter, D_{int} and D_{ac} are the inter-valley and acoustic deformation potential constants, respectively, c_1 is the longitudinal sound velocity, and $\hbar\omega_{\nu\nu'}$ is the phonon energy involved in inter-valley scattering (Einstein approximation $\hbar\omega_{\nu\nu'} = \hbar\omega_0$ used). The elastic approximation for the acoustic-phonon scattering rate and the equipartition approximation for the acoustic-phonon occupation probabilities have been applied, i.e. $f_B[\vec{q}] \approx k_B T_L / \hbar c_1 |\vec{q}|$. Effective mobilities and effective electric fields are computed in analogy to bulk MOSFETs:

$$\mu_{\text{eff}} = \frac{\int dz \mu[z] n[z]}{\int dz n[z]},$$

$$E_{\text{eff}} = \frac{\int dz |\hat{z} \cdot \vec{E}[z]| n[z]}{\int dz n[z]},$$

where \hat{z} denotes the unit normal vector along quantization direction z , and the interface positions are chosen as integration limits.

3. Simulation Results

Figure 4 shows μ_{eff} versus E_{eff} for the symmetrical DGSOI ($t_{\text{ox}} = t_{\text{box}} = 2 \text{ nm}$). In ultra-thin Si films with $t_{\text{Si}} < 4 \text{ nm}$ the mobility is suppressed due to geometrical confinement. An enhancement w.r.t. to the bulk curve is observed at intermediate and strong fields around $t_{\text{Si}} \approx 10 \text{ nm}$ (compare Fig. 3). The phonon-limited effective mobility as function of t_{Si} shown in Fig. 5 serves to explain the behavior in the different t_{Si} -regions in case of the symmetrical DGSOI. The phonon-limited bulk values are reached for $t_{\text{Si}} > 15 \text{ nm}$, when the interaction between upper and lower channel gradually disappears due to the growing potential barrier that separates the two inversion layers. The broad maxima around $t_{\text{Si}} \approx 10 \text{ nm}$ are caused by the so-called volume inversion. As extensively discussed in Refs. [1], [4], in this region the communication between the two channels is associated with a reduction of the form factors $\alpha_{N'N}$ and, therefore, leads to an enhancement of

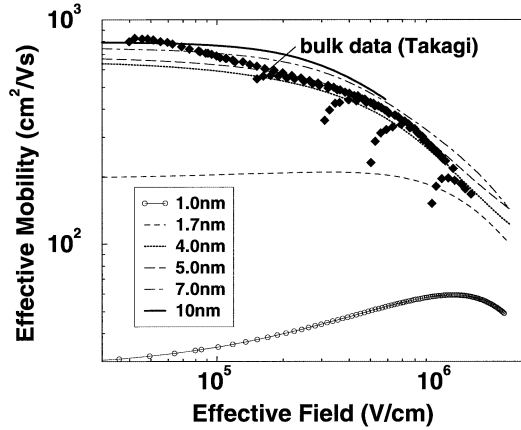


Fig. 4 Effective mobility versus effective field for $t_{ox} = t_{box} = 2$ nm, and various t_{Si} . Bulk data [12] are shown for comparison.

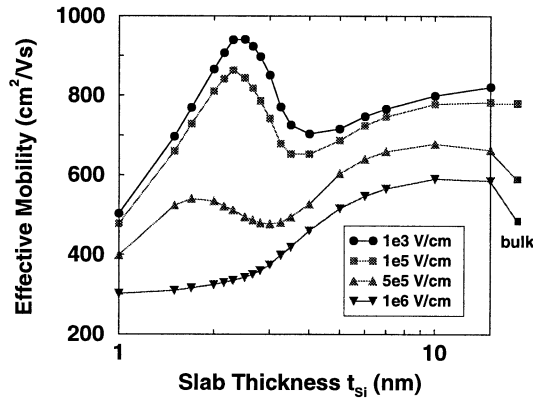


Fig. 5 Phonon-limited effective mobility versus SOI thickness for $t_{ox} = t_{box} = 2$ nm, and various E_{eff} . IR scattering was switched off.

the mobility compared to the corresponding bulk MOSFET. The latter was obtained from the DGSOI by removing the buried oxide and changing the n^+ back-gate into a p-type substrate. Decreasing the Si thickness, the region governed by geometrical confinement starts at $t_{Si} \approx 4$ nm. At low and intermediate effective fields, the mobility first sharply increases, since the average conductivity mass is reduced by the stronger population of the lowest non-primed ladder. With further reduction of t_{Si} the growth of the form factors dominates over sub-band splitting and population effects and the mobility sharply drops. However, the range $t_{Si} < 4$ nm is of academic interest only, because it is (currently) inaccessible by technology, and because IR scattering drops the mobility below its bulk values in this region. This is demonstrated in Fig. 6, where IR scattering now is included. As can be seen, the mobility enhancement around $t_{Si} = 10$ nm has survived, although reduced in size and at a much lower mobility level. These changes obviously depend on the choice of the IR parameters.

For the mobility enhancement it is essential that two equally filled channels can form. This is impossible

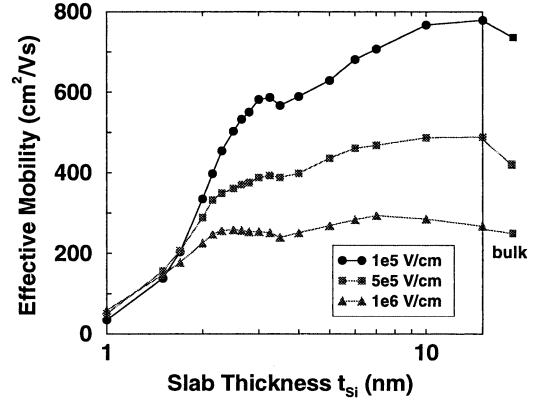


Fig. 6 Effective mobility with IR scattering versus SOI thickness for $t_{ox} = t_{box} = 2$ nm, and various E_{eff} .

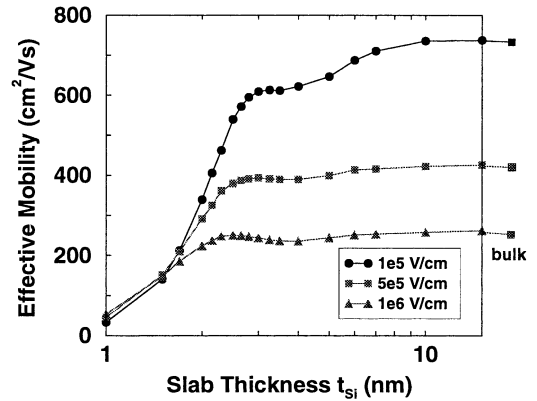


Fig. 7 Effective mobility with IR scattering versus SOI thickness for $t_{ox} = 2$ nm, $t_{box} = 200$ nm, and various E_{eff} .

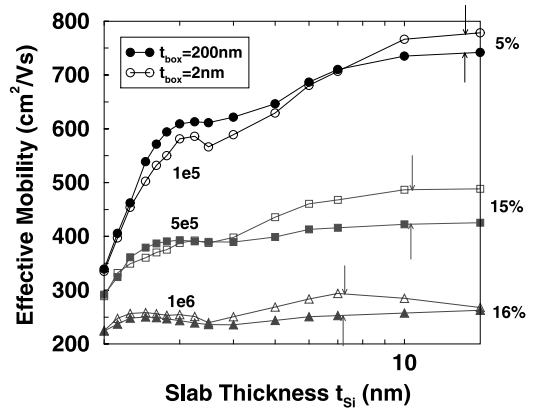


Fig. 8 Effective mobility with IR scattering versus SOI thickness for $t_{ox} = 2$ nm and various E_{eff} and t_{box} .

in the more realistic case of a thick buried oxide. The results in Fig. 7 for $t_{box} = 200$ nm show that the mobility enhancement vanishes. This case is almost identical to single-gate SOI MOSFETs, where practically no mobility enhancement was found [4].

Figure 8 compares the symmetrical with the asymmetrical device. For our choice of Δ_2 and L_{corr2} , the

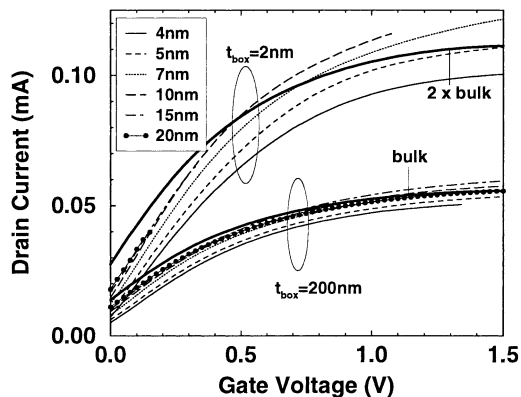


Fig. 9 Transfer characteristics at $V_{DS} = 1$ mV for various t_{Si} .

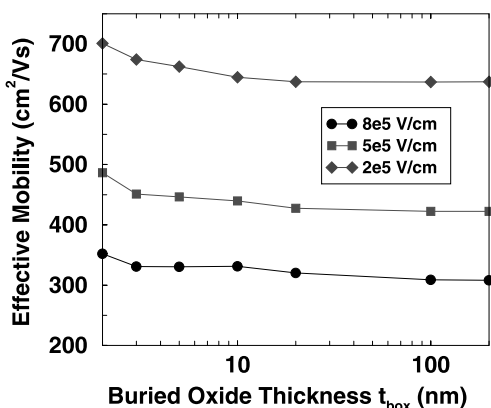


Fig. 10 Decrease of the effective mobility towards its bulk values with increasing t_{box} for various E_{eff} ($t_{Si} = 10$ nm, $t_{ox} = 2$ nm).

difference amounts to 6% at $E_{eff} = 1 \times 10^5$ V/cm and to 15–16% under strong inversion. These numbers also roughly represent the effect in comparison to the bulk MOSFET.

The transfer characteristics in Fig. 9 confirm these results. In the symmetrical case the on-current exceeds two times the current of a bulk MOSFET (two parallel channels!). At $V_{GS} = 1$ V a 8% enhancement on top of that is observed for the 10 nm SOI candidate. However, in the case of $t_{box} = 200$ nm there is only one channel left, and due to the absence of volume inversion the mobility can only gradually approach the bulk value, but not exceed it.

In order to demonstrate the loss of volume inversion with growing buried oxide, we plotted the effective mobility as a function of t_{box} in Fig. 10. An increase of t_{box} by a few nm is sufficient to halve the enhancement. Figure 11 explains the situation in terms of band edge and density. The density in the upper channel is almost unaffected by an increase of t_{box} , whereas the lower channel vanishes.

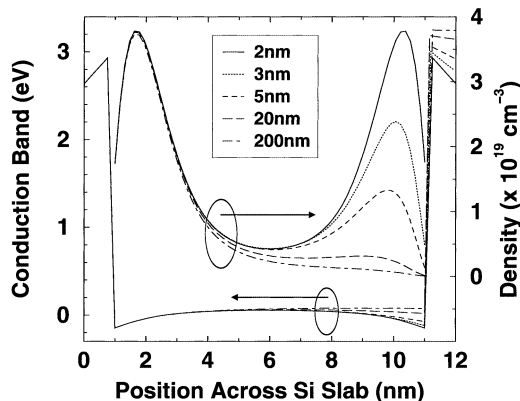


Fig. 11 Conduction band profile (left) and electron density (right) across the Si slab for various t_{box} ($t_{Si} = 10$ nm, $t_{ox} = 2$ nm, $V_{GS} = 1$ V).

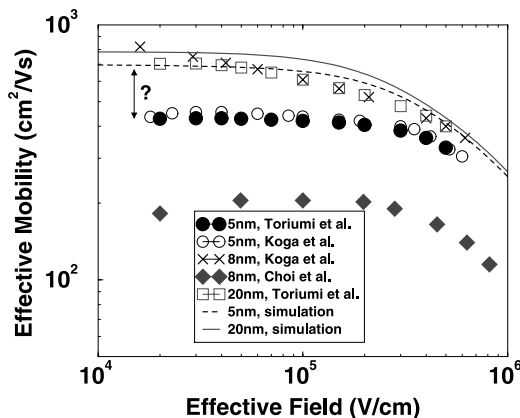


Fig. 12 Comparison with experimental data. Parameters: $\Delta_1 = \Delta_2 = 0.32$ nm.

4. Comparison with Measurements

A comparison with (rare) experimental data [13]–[15] is shown in Fig. 12. For these simulations, t_{ox} and t_{box} were adapted to the published values. Most striking is the discrepancy for the 5 nm SOI (700 cm²/Vs simulated versus 420 cm²/Vs measured), since one would expect the mobility to be phonon-limited in this range. The open circles are very recent data from a sample with ‘poor’ buried interface [15] (measured density of interface traps $D_{it} = 6 \times 10^{11}$ cm⁻²eV⁻¹). For comparison, the same group measured a sample with $t_{Si} = 8$ nm (crosses), where the buried interface had a much higher quality ($D_{it} = 4 \times 10^{10}$ cm⁻²eV⁻¹). For the same t_{Si} , older data [14] are significantly lower (diamonds). This shows the dramatic influence of the quality of the buried interface on the effective mobility. Koga et al. [15] attributed the mobility degradation in case of the ‘poor’ buried interface to Coulomb scattering at charged interface states.

5. Conclusion

We have implemented a mobility model based on the numerical solution of the 1D-Schrödinger equation into the device simulator DESSIS-ISE. Convergence is improved by a hybrid technique, where the whole device is simulated with the density-gradient model, and only the channel mobility is computed with the information from the Schrödinger window. We showed that the volume-inversion related enhancement of μ_{eff} for $t_{\text{Si}} \approx 10$ nm only occurs in symmetrical DGSOIs. Thick buried oxides, as present in today's SIMOX technology, prevent the inversion of the buried channel and limit μ_{eff} to the bulk value. The comparison with published experimental data is still hampered by the immature technology.

References

- [1] M. Shoji and S. Horiguchi, "Electronic structures and phonon-limited electron mobility of double-gate silicon-on-insulator Si inversion layers," *J. Appl. Phys.*, vol.85, no.5, pp.2722–2731, March 1999.
- [2] S. Takagi, J. Koga, and A. Toriumi, "Mobility enhancement of SOI MOSFETs due to subband modulation in ultra-thin SOI films," *Ext. Abstracts SSDM*, pp.154–155, Hamamatsu, 1997.
- [3] F. Gámiz, J.B. Roldán, P. Cartujo-Cassinello, J.E. Carceller, J.A. López-Villanueva, and S. Rodriguez, "Electron mobility in extremely thin single-gate silicon-on-insulator inversion layers," *J. Appl. Phys.*, vol.86, no.11, pp.6269–6275, Dec. 1999.
- [4] F. Gámiz and M.V. Fischetti, "Monte Carlo simulation of double-gate silicon-on-insulator inversion layers: The role of volume inversion," *J. Appl. Phys.*, vol.89, no.10, pp.5478–5487, 2001.
- [5] F. Gámiz, J.B. Roldán, J.A. López-Villanueva, P. Cartujo-Cassinello, and J.E. Carceller, "Surface roughness at the Si-SiO₂ interfaces in fully depleted silicon-on-insulator inversion layers," *J. Appl. Phys.*, vol.86, no.12, pp.6854–6863, Dec. 1999.
- [6] A. Wettstein, O. Penzin, and E. Lyumkis, "Integration of the density gradient model into a general purpose device simulator," *VLSI Design*, vol.15, no.4, pp.751–759, 2002.
- [7] A. Wettstein, *Quantum Effects in MOS Devices*, vol.94, Series in Microelectronics, Hartung-Gorre, 2000.
- [8] A. Schenk, "Physical modeling of deep-submicron devices," *Proc. 31th ESSDERC'01*, pp.9–16, 2001.
- [9] ISE Integrated Systems Engineering AG, *DESSIS 8.0 Reference Manual*, 2002.
- [10] S.M. Goodnick, D.K. Ferry, C.W. Wilmsen, Z. Liliental, D. Fathy, and O.L. Krivanek, "Surface roughness at the Si(100)-SiO₂ interface," *Phys. Rev. B*, vol.32, no.12, pp.8171–8186, Dec. 1985.
- [11] G. Masetti, M. Severi, and S. Solmi, "Modelling of carrier mobility against carrier concentration in arsenic-, phosphorus- and boron-doped silicon," *IEEE Trans. Electron Devices*, vol.ED-30, no.7, pp.764–769, 1983.
- [12] S. Takagi, A. Toriumi, M. Iwase, and H. Tango, "On the universality of inversion layer mobility in Si MOSFET's: Part I—Effects of substrate impurity concentration," *IEEE Trans. Electron Devices*, vol.41, no.12, pp.2357–2362, Dec. 1994.
- [13] A. Toriumi, J. Koga, H. Satake, and A. Ohata, "Performance and reliability concerns of ultra-thin SOI and ultra-thin gate oxide MOSFETs," *IEDM*, pp.847–850, IEEE, 1995.
- [14] J.-H. Choi, Y.-J. Park, and H.-S. Min, "Electron mobility behavior in extremely thin SOI MOSFETs," *IEEE Electron. Device Lett.*, vol.16, no.11, pp.527–529, 1995.
- [15] J. Koga, S. Takagi, and A. Toriumi, "Influences of buried-oxide interface on inversion-layer mobility in ultra-thin SOI MOSFETs," *IEEE Trans. Electron Devices*, vol.49, no.6, pp.1042–1048, June 2002.



Andreas Schenk was born in 1957. He received the Dipl. Phys. degree and the Ph.D. from Humboldt University in Berlin (HUB) in 1981 and 1987, respectively. From 1987 till 1991 he was working on various aspects of the physics and simulation of optoelectronic devices. In 1991 he joined the Integrated Systems Laboratory of ETH working as a senior research/teaching assistant, where he qualified to give lectures at university in 1997

for "Physics and Modeling of Microelectronic Devices." His main activities are in the physics-based modeling for advanced simulation of sub-micron silicon devices and their application in the TCAD software released by ISE AG Zurich. His interests include generation-recombination, mobility, contacts, heterojunctions, many-body effects, hot carrier degradation, noise, single electron transistor modeling at device level, and quantum effects in silicon ultra-small devices. He authored and co-authored 2 books and 80 papers. Andreas Schenk is a member of the German Physical Society (DPG).



Andreas Wettstein received the diploma in physics from the Universität Karlsruhe in 1995 and the Ph.D. degree in engineering from the Eidgenössische Technische Hochschule in Zürich in 2000. Since then he is with ISE AG, Zürich, working as a software developer for device simulation.